Check for updates

Experimental Demonstration of In-Memory Computing in a Ferrofluid System

*Marco Crepaldi, Charanraj Mohan, Erik Garofalo, Andrew Adamatzky, Konrad Szaciłowski, and Alessandro Chiolerio**

Magnetic fluids are excellent candidates for several important research fields including energy harvesting, biomedical applications, soft robotics, and exploration. However, notwithstanding relevant advancements such as shape reconfigurability, that have been demonstrated, there is no evidence for their computing capability, including the emulation of synaptic functions, which requires complex non-linear dynamics. Here, it is experimentally demonstrated that a Fe_3O_4 water-based ferrofluid (FF) can perform electrical analogue computing and be programmed using quasi direct current (DC) signals and read at radio frequency (RF) mode. Features have been observed in all respects attributable to a memristive behavior, featuring both short and long-term information storage capacity and plasticity. The colloid is capable of classifying digits of a 8×8 pixel dataset using a custom in-memory signal processing scheme, and through physical reservoir computing by training a readout layer. These findings demonstrate the feasibility of in-memory computing using an amorphous FF system in a liquid aggregation state. This work poses the basis for the exploitation of a FF colloid as both an in-memory computing device and as a full-electric liquid computer thanks to its fluidity and the reported complex dynamics, via probing read-out and programming ports.

1. Introduction

As a part of the largest international effort underway to explore alternative computing methods called *unconventional computing*,[1,2] there is a consolidated trend in the research on devices, materials, and in natural processes, to find an implicit exhibition of computing features, even beyond solid aggregation state. The idea of computing with liquids attracted engineers and mathematicians since the early 1900s,[3] but later prototypes of liquid computers were mostly based on hydraulic, reaction-diffusion, and fluidic principles,[4] with the drawback of requiring either a continuous movement of the liquid, or a "reloading" operation after its potential/chemical energy was consumed.

Only recently, liquid and colloidal systems have been subject to attention for mimicking the ions moving in the human brain through embedding aqueous solutions in gel or solid-state scaffolds.[5] Being applicable to soft robotics,[6] energy harvesting,[7] and computation in general,[8] magnetic fluids are always of great research interest (Section S1, Supporting Information). Particularly, ferrofluids (FFs) are mixtures in which nanometric-size dispersed insoluble particles are suspended throughout a solvent, the particles being typically superparamagnetic, giving rise to interesting collective behavior. One of the most interesting properties of colloids, is their ability of being potentially fault tolerant, resilient, and robust to failures of various nature. Colloids, are excellent examples of how matter can self organize, with their nanoparticles that form bulk phases such as liquid and crystals and provide collective behavior not seen at atomic scale.[9] A potential of FF in computing, massive-parallel information processing, sensing, and energy harvesting regardless of their shape has not been addressed

M. Crepaldi, C. Mohan
Electronic Design Laboratory
Istituto Italiano di Tecnologia
Via Melen 83, Genova, Liguria 16152, Italy

E. Garofalo, A. Chiolerio
Bioinspired Soft Robotics
Istituto Italiano di Tecnologia
Via Morego 30, Genova, Liguria 16163, Italy
E-mail: alessandro.chiolerio@iit.it

A. Adamatzky, A. Chiolerio
Unconventional Computing Laboratory
University of West England
Frenchay Campus
Coldharbour Ln, Bristol, Bristol BS16 1QY, UK

K. Szaciłowski
Academic Centre for Materials and Nanotechnology
AGH University of Technology
30 Mickiewicza Avenue, Kraków 30-059, Poland

2211406 (1 of 10)

© 2023 The Authors. Advanced Materials published by Wiley-VCH GmbH

**ADVANCED
SCIENCE NEWS**

www.advancedsciencenews.com

**ADVANCED
MATERIALS**

www.advmat.de

before, notwithstanding first reports on their shape reconfiguration are already available.[10] Here, we demonstrate that a volume of a superparamagnetic FF can be interchangeably assigned to memory and computing roles. This property is consistent with the rising paradigm of in-memory computing, which aims at mitigating processor-memory data transfer bottleneck by embedding computation in memory.[11–14] We show that a FF can run digit classification, and be considered as a liquid in-memory computing device in a two port set-up. Moreover, as a natural consequence of its complex dynamics combined to its amorphous nature and fluidity, a FF reservoir can be considered equivalent to a physical in-memory computer, an ensemble of computing nodes shaped by the number of physical ports for programming and read-out. In-memory computing paradigm is currently applied to solid state computer architectures, and it is implemented using digital computer logic and charge carrier-based memories or by integrating specific resistance-based memristive devices on it.[14] In-memory computing using memristive devices is always obtained in conjuction with spiking and non-spiking neural networks routed in solid state circuits. These solid-state devices are typically integrated in geometrically arranged cross-bars to implement a wide variety of computation primitives such as non-stateful/stateful logics and matrix multiplication, fundamental elements to map computer instructions directly where information storage occurs.[14] Cross-bars of analog devices are also feasible, since they can be interfaced with solid-state logics using analog-to-digital and digital-to-analog converters.[15] On the other hand, an FF constitutes itself a network of in-memory computing elements, the nanoparticles, that can be arbitrarily probed by programming and read-out ports thanks to its fluidity. Further, nanoparticles are subject to electromagnetic forces that can alter their location, speed magnitude and direction, therefore modifying the connection scheme of said network. In solid-state systems, a digit classification task is considered as a high-level application, and ad hoc architectures are typically based on the co-design of devices with associated neural network, that can include multiple layers.

Here, we demonstrate that the FF is an in-memory computer by itself, by providing inputs using a specific sequence of voltage stimuli over time. We herein aim at demonstrating basic computing features, and given the long colloid system timescales, we used a custom 8×8 digit dataset to demonstrate basic in-memory computing functionality. To further verify its dynamical properties, we demonstrate FF computation using the concept of reservoir computing (RC), a paradigm that takes advantage from system dynamics (spontaneous or excited from external sources) for advanced information processing. Reversibility, fading memory, nonlinearity of electrical response and structural stochasticity are usually considered as prerequisites for any physical implementation of RC concepts,[16] and most solid-state memristors fulfill these requirements.[17]

2. Experimental Set-Up and Hysteresis

We aim at demonstrating the basic computing properties of an FF system, in particular using a set-up featuring two terminals, in view of an extension with a larger number of ports, distributed over the entire volume of FF reservoir, as detailed in Section 5. Our experimental setup shown in **Figure 1**A comprises an FF

sample (the reservoir) connected to a two-port vector network analyzer (VNA), a direct current (DC) bias generator (where the negative terminal is internally connected to ground) and two bias tee circuits to decouple radio frequency (RF) and DC signals. Both the DC bias generator and the VNA are connected to a personal computer to implement measurement scripts (Section S2, Supporting Information), that is, applying a DC voltage across the reservoir and reading the impedance through its S-parameters, that can be always converted to impedances as a function of frequency. As shown in Figure 1B, the FF is stimulated as follows: a quasi-DC voltage V_P (bipolar) is applied to the system to program/write it, and its internal status (read) is acquired in RF mode using the magnitude impedance parameters. Since the observed S-parameters and consequently impedance magnitude variations are small (Section S3, Supporting Information), the sum of the numerical impedance values over all scanned frequencies Z_{xy}^C can be used profitably as an indicator of the internal status of the reservoir (see the formulas in the figure). This way the S-parameters are collapsed into a single number for each measurement point, reducing data volume 100 folds, and enabling specialized electronics to read the liquid status without requiring any accurate sub-systems (see Section S15, Supporting Information). Consequently, each reading measurement is an ensemble of four real numbers Z_{11}^C, Z_{12}^C, Z_{21}^C, and Z_{22}^C, all of those being a function of time t, for example, for port one, $Z_{11}^C \equiv Z_{11}^C(t)$. Such approach is chosen to test the robustness of liquid state programming, coding and computing: in fact the algebraic sum of all impedance values does not represent any optimal choice of a specific working point that might provide higher rejection/amplification/signal-to-noise ratio (see e.g., Figure S1, Supporting Information, @ 1 GHz).

Hysteresis, a fingerprint of memristance,[18] is a necessary condition for neuromorphic computation.[19] Figure 1C shows hysteresis loops obtained performing a voltage sweep from −3.8 to 3.8 V with steps of 0.1 V each lasting 1 s, repeated for 50 times. At the beginning of the test ($t = 0$ s) we started with $V_P = -0.85$ V and impedance values were $Z_{11}^C(0) = 14312\ \Omega$, $Z_{12}^C(0) = 2320\ \Omega$, $Z_{21}^C(0) = 2060\ \Omega$, and $Z_{22}^C(0) = 11795\ \Omega$. The pinched hysteresis of Z_{11}^C shrinks for positive V_P as the number of iterations increases, even with such zero average excitation. The hysteresis of Z_{22}^C shrinks throughout the whole V_P range while for Z_{12}^C and Z_{21}^C we observe the opposite phenomenon. On the one hand, the results indicate that assuming a given DC stimulus, its effect on the impedance variation is not constant and varies over time. On the other hand, this feature indicates a long-term adjustment of the material toward an *equilibrium* condition, that can be interpreted as the feature of memorizing the previous DC bias history. Furthermore, due to fluidity of the material, this memory will be naturally fading, which is another important prerequisite for an efficient and universal RC system.[20]

3. Information Storage

The liquid can be used to store information in the form of a particular impedance evolution at a given port. To pose a parallelism with biological neurons we can refer to a *long-term plasticity* feature. **Figure 2**A shows the stimulus scheme used to demonstrate storage capacity for N information values—in this specific test
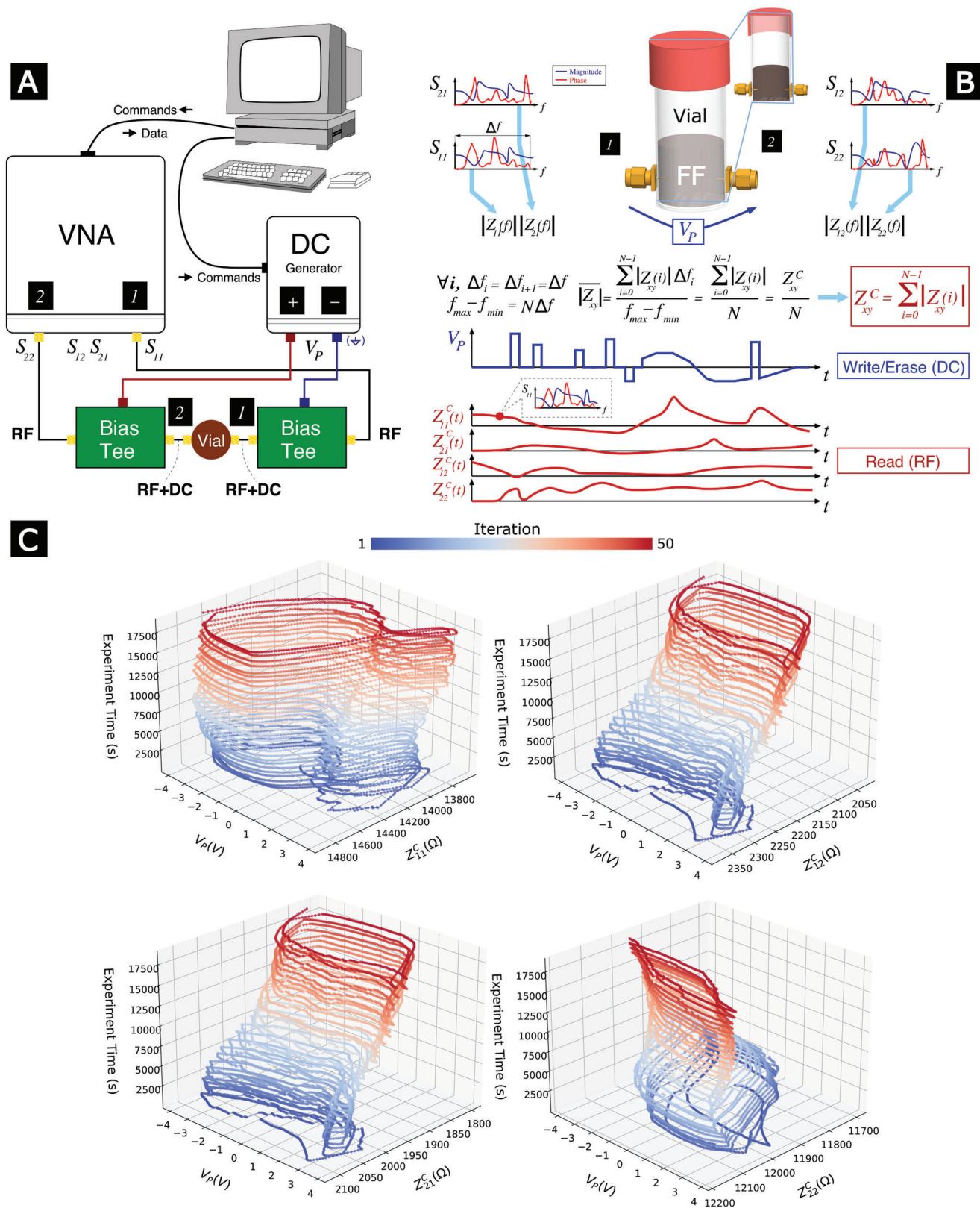
Figure 1. A) Experimental set-up. B) Measurement concept and relevant parameters. The colloid is programmed using a quasi-DC voltage and its internal status is read through its distributed impedance values Z_{11}^C, Z_{12}^C, Z_{21}^C, and Z_{22}^C, that correspond to the sum of the impedance values obtained throughout the measurement bandwidth of the VNA (10 MHz–6 GHz). C) Hysteresis loops as a function of experiment elapsed time obtained from an initial impedance multi-point (comprising Z_{11}, Z_{12}, Z_{21}, and Z_{22}), recorded by applying a −3.8–3.8 V voltage sweep.
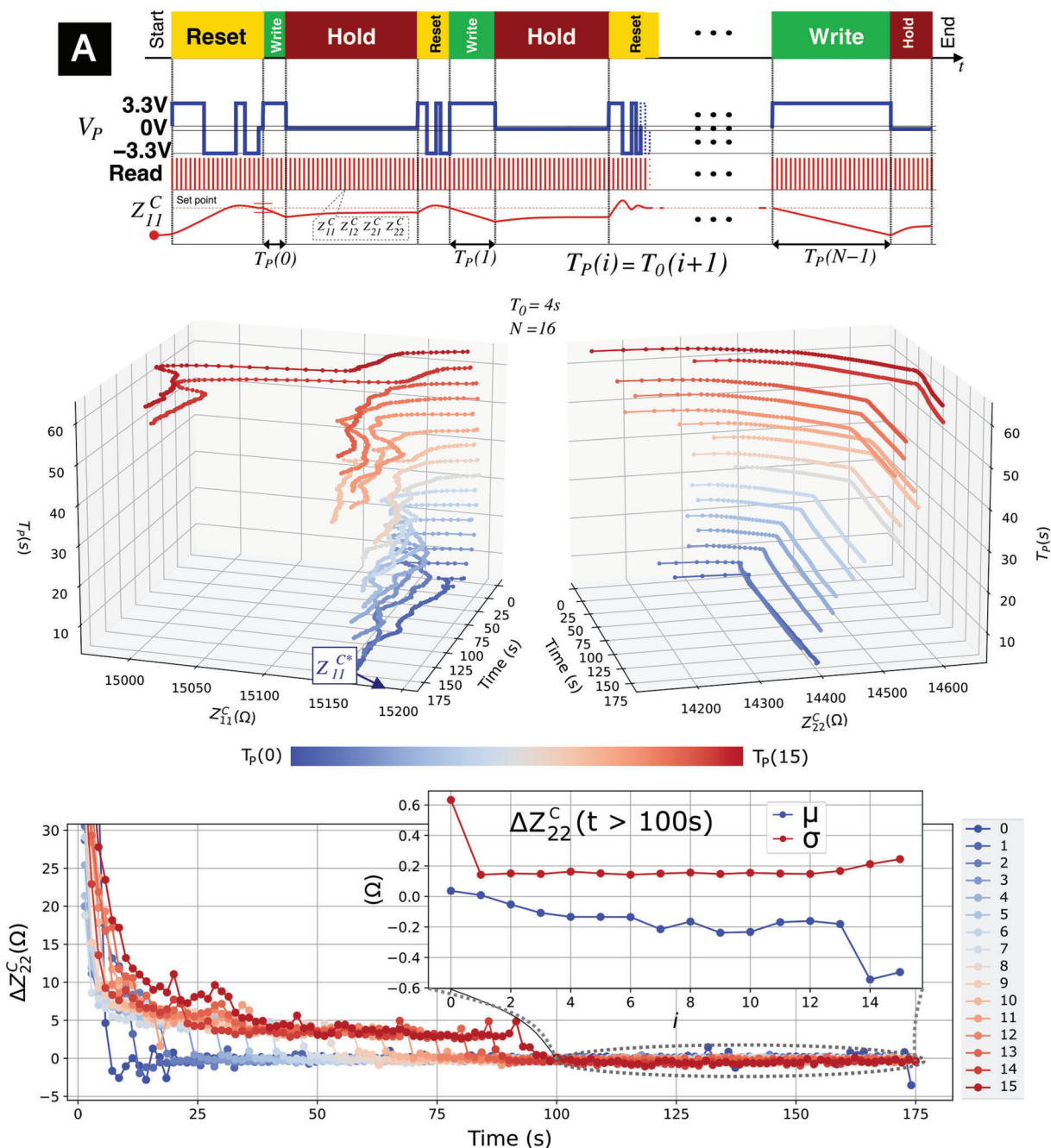
Figure 2. A) Long-term memory stimulus scheme and B) results obtained by applying a positive pulse to the material of amplitude 3.3 V with different duration $T_P(i)$, and by restoring the initial impedance value $Z_{11}^{C*} = 14338\ \Omega$ for each test using a closed control loop. C) Variation of Z_{22}^C and corresponding mean and variance during the Hold phase for all information values.

$N = 16$. The test comprises repeated Reset, Write and Hold phases, where Reset implements a control loop on Z_{11}^C to reset its value to Z_{11}^{C*}. The results in Figure 2B show that Z_{11}^{C*} is correctly set for each iteration, and notwithstanding impedance control is implemented at port one, Z_{22}^C evolves toward well defined impedance values, that are a function of the applied pulse duration $T_P(i)$. Interestingly, the Z_{22}^C values do not reset at the beginning of each Write phase. The small variation of ΔZ_{22}^C values and the associated uniform distribution parameters during Hold

of Figure 2C, suggest that the colloid can be used as a high resolution short-term memory. In general, as $T_P(i)$ can be controlled with the power of continuum, analogue information storage can be implemented and information can be stored even for a longer duration (Section S4, Supporting Information). In general, losses depend on the working point selected along the hysteresis loop, and information storage can be achieved with pulses featuring proportional amplitude. However, results in Section S4, Supporting Information show that given the complex dynamics of the FF,

**ADVANCED
SCIENCE NEWS**

www.advancedsciencenews.com

**ADVANCED
MATERIALS**

www.advmat.de

pulse-width programming can be considered more effective assuming a maximum voltage of 3.3 V, compliant with standard electronic components.

4. Computing

4.1. Pattern Classification

By extending the memory stimulus scheme of Figure 2A, we could demonstrate in-memory digit classification. To this end, we prepared a dataset consisting of the ten digits 0–9, in 8×8 matrices of pixels (Section S5, Supporting Information), that we have transformed into a linear time sequence of stimuli (serialized) as shown in the scheme of **Figure 3**A. Data serialization has been demonstrated to be an efficient approach toward neuromorphic data processing with very minimal computational resources (e.g., single artificial neurons[21,22]). Each pixel, besides its value 0–1 that can be mapped to a voltage level V_P, can be attributed a weight in terms of pulse duration w_i and, in general, an offset (in terms of additive voltage). It is therefore possible to build up sequences with higher or lower sensitivity to a particular digit or selectively filter particular pixel values. The resulting weight matrix given an expected digit, can be computed by simply assigning longer duration to the expected black pixels of that given digit, so that the liquid dynamics is exacerbated. In turn, when digits are "submitted" to the sample, in presence of the expected digit (the one that was predefined), impedance variation is usually higher, if compared to other non-expected digits (non-predefined). Such property is used for digit matching. Here, we do not bias the colloid in the condition of having a pinched hysteresis, so to obtain a monotonic decrease of impedance during the tests, and therefore enable a direct comparison of the final value for all digits after the application of the sequences. By assuming instead that the system is in the conditions of a pinched hysteresis, the FF can progressively adapt to implement a learning mechanism by providing a particular non-zero offset weighting (Section S6, Supporting Information).

Figure 3B shows the stimulus scheme of the pattern classification test, which exploits in-memory computing features. Similarly to the memorization experiments, here we apply a reset control sequence on Z_{22}^C, toward the impedance set-point $Z_{22}^C = 14338\ \Omega$, using an initial `Charge` phase at 10 V. Each pixel is associated to a -3.3 or 0 V voltage (black or white) for a given weight duration, with zero offset. After verifying differentiation (Section S5, Supporting Information), we provide the weighted sequences, so that the pulse duration of each expected black pixel is longer when compared to the others. We apply sequentially all serialized pixel matrices from 0 to 9, using all the weighted sequences for each digit. Figure 3C–E shows the measurement results assuming 4.5 and 0.5 s weights (black and white, respectively), for three sample digits, 1, 4, and 7. Results show that with this in-memory computing scheme Z_{22}^C decreases more considerably in case the weighted sequence matches the predefined digit. The final match can then be achieved by applying a simple threshold on the Z_{22}^C value, which depends on the digit to be detected, or alternatively, by indexing the digit that leads to the lowest impedance. This particular scheme fails for 3 which is a subset of 8 (Figure 3F), thus leading to an overall 90% accuracy. As an effect of long-term plasticity, we have also observed

that if the above test is repeated for days without interruption, the impedance dynamics shrinks, irrespective of the digit (see Section S7, Supporting Information). We have qualitatively observed through experiments, however, that the behavior of the liquid is reversible and that impedance dynamics can be restored. By progressively injecting small quantities of FF in the reservoir, and therefore dynamically changing its volume, we demonstrated that the FF can be successfully scaled to run in-memory computing at different volumes. This can be done by setting different initial impedance conditions depending on the volume of liquid (Section S13, Supporting Information). This result implicitly demonstrates that the liquid computer is scalable. We have observed also that the responsiveness of the material increases for larger temperatures, and initial impedance conditions need to be adapted also in this context.

4.2. Physical Reservoir Computing

Similarly to solid-state memristors (see also detailed comparison in Section S8, Supporting Information), to further demonstrate the computation capability of the FF, we have implemented PRC using an ad hoc readout layer. The FF exhibits chaotic nature (resulting inter alia from Brownian motions as well as from the surfactant molecules featuring electrical polarizability), and within its deterministic features, it presents a strong sensitivity to initial electrical conditions (Section S9, Supporting Information), while it can provide both fading memory and long-term plasticity (for instance see the plots in Figure S3, Supporting Information). RC is typically implemented taking advantage of a physical reservoir short-term memory.[23] However, within the time frame of a digit classification, our findings show that the dynamics of the FF tend to shrink in the long-term if a trivial reset condition is used (Section S7, Supporting Information). Moreover, besides sensitivity to initial conditions, the FF exhibits chaotic non-equilibrium at repeated impedance sets (Section S10, Supporting Information). As a further confirmation of its complex dynamics, repeated programming sets and resets lead to high variability, without dedicated countermeasures. While a trivial initial impedance control is necessary to achieve repeatability of in-memory computing, over the long term it is not enough to avoid dynamics shrinking, and other countermeasures must be put in place, as here described. Such features can make PRC unfeasible and it is thus necessary to avoid changes in dynamical regime during both training and inference. To mitigate these variations and solve this issue, we have designed a particular "reset" sequence that maintains the dynamical features of the material consistent. It features the application of a high voltage toward two impedance points that are higher and lower compared to the initial impedance Z_{22}^{C*} used to run active computation, respectively. **Figure 4**A shows the measurement scheme and the reset sequence. In our tests $Z_{22}^C|_{LOW} = 16350\ \Omega$, $Z_{22}^C|_{HIGH} = 16450\ \Omega$, and $Z_{22}^{C*} = 16400\ \Omega$.

We used the same in-memory computing scheme given in Figure 3A and constant weighting to serialize the 64 pixels of the digit matrices (each pixel lasts 2 s, with -3.3 V for 1 and 0 V for 0) and we have trained a neural network (NN) layer to classify four digits 0–3 using a training dataset comprising 200 digits, (50×4, rationale and dataset presented in Section S11, Supporting Information). The NN comprises a first block which
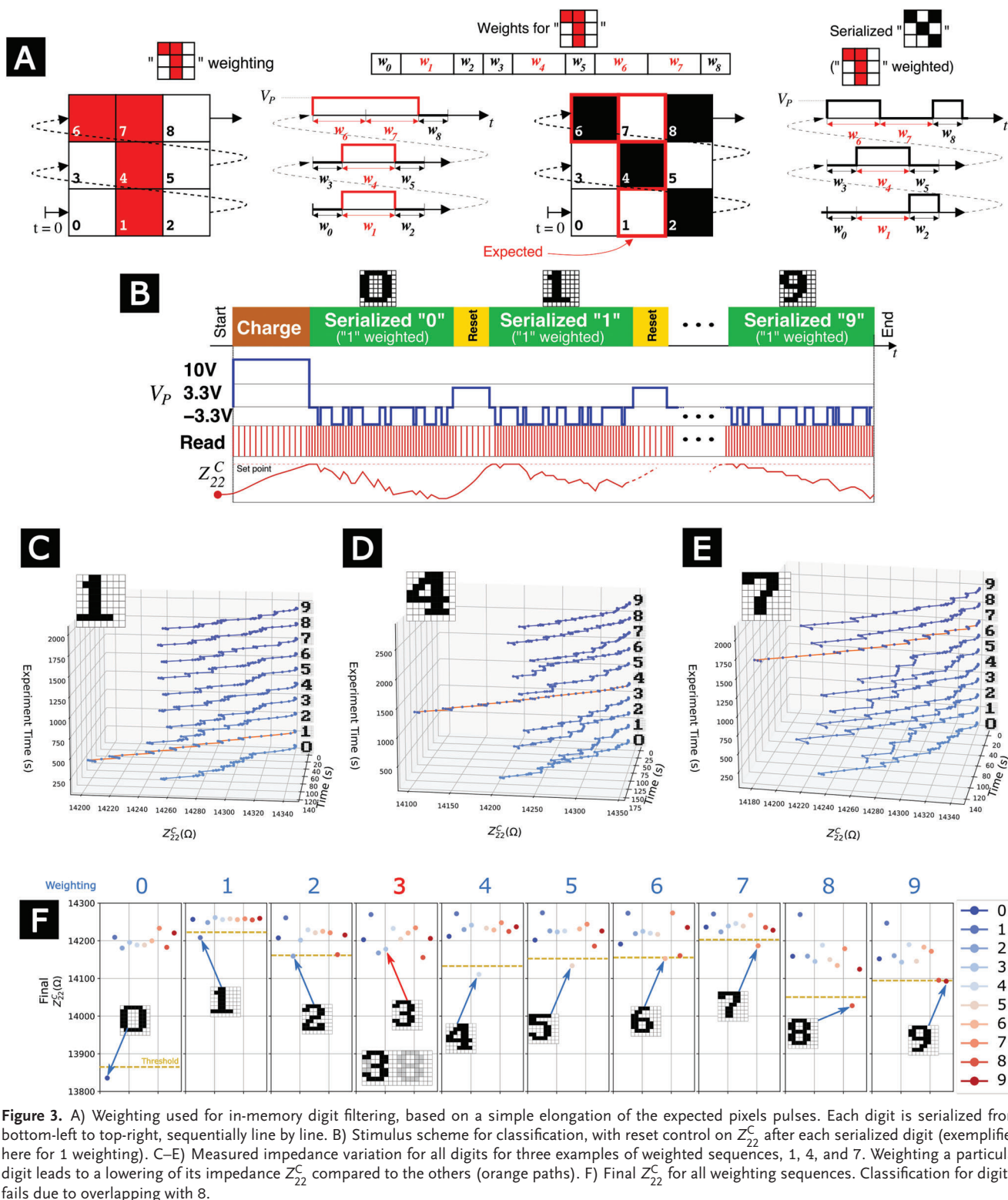
Figure 3. A) Weighting used for in-memory digit filtering, based on a simple elongation of the expected pixels pulses. Each digit is serialized from bottom-left to top-right, sequentially line by line. B) Stimulus scheme for classification, with reset control on Z_{22}^C after each serialized digit (exemplified here for 1 weighting). C–E) Measured impedance variation for all digits for three examples of weighted sequences, 1, 4, and 7. Weighting a particular digit leads to a lowering of its impedance Z_{22}^C compared to the others (orange paths). F) Final Z_{22}^C for all weighting sequences. Classification for digit 3 fails due to overlapping with 8.

2211406 (6 of 10)

**ADVANCED
SCIENCE NEWS**

www.advancedsciencenews.com
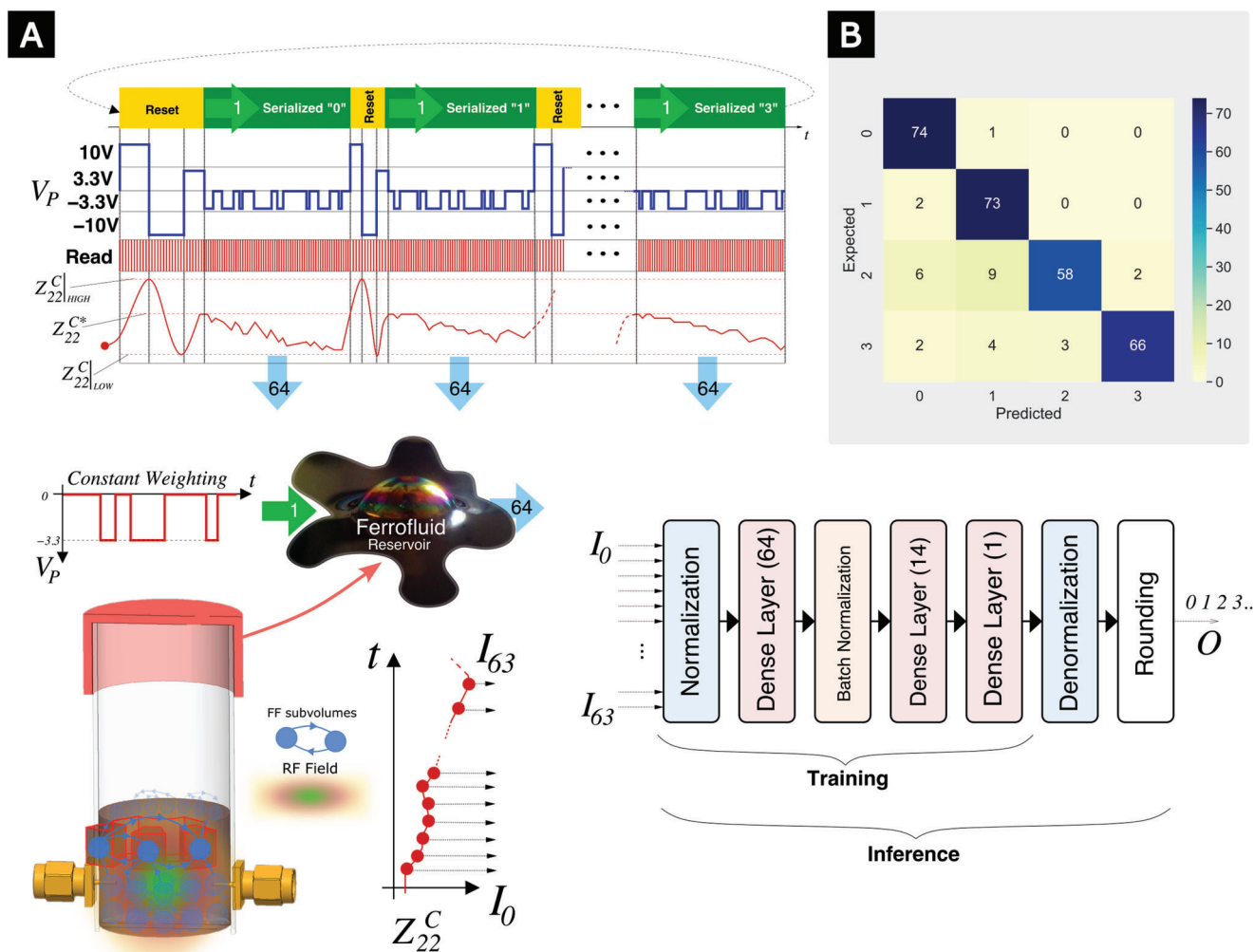
**ADVANCED
MATERIALS**

www.advmat.de

Figure 4. A) Stimulus scheme used for both training and inference during PRC tests with parallelized outputs for the readout NN layer (each one identifying the effect of a pixel value), detail on the NN layer and conceptual liquid reservoir. B) Confusion map of a real-time classification test of the digits 0 to 3 using the trained NN.

normalizes in parallel the 64 impedance values in the range 0–1 to get rid of residual dynamical variations due to the FF chaotic nature. The input layer is made of a 64 `Dense` model, followed by a `Batch Normalization` block (that helps back-propagation convergence), another 14 elements `Dense` model, and finally a single `Dense` neuron. Inference is achieved in real-time using the trained NN on new measurement data from the FF consisting of 64 impedance values Z_{22}^C. Figure 4B shows the confusion map associated to the detection of 300 new digits, after detecting the four digits with the pre-trained NN, achieving an accuracy of 90.6%.

5. Discussion, Conclusions, and Future Prospects

In this work, we have demonstrated a neuromorphic device that operates solely on the basis of liquid state matter, showing complex switching dynamics, memory features, and capable of advanced neuromorphic information processing. Few former literature reports on liquid state memristors exist, most of which are liquid because of the use of liquid InGa alloy as electrodes[24]

or ionic liquid as a medium, in which metallic conductive filaments are formed.[25] For all formerly reported devices, however, only basic learning functionality has been demonstrated, for example, hysteresis loop and on/off switching. Literature reports indicate the possibility of scaling liquid state memristors down to nanoscale (30 nm size of the liquid well) providing that nonvolatile solvents are used.[25]

In this work, we have demonstrated scaling capability with a large volume of liquid of a complex nanoparticle colloidal suspension. The choice of magnetite is driven by its sustainable features: it is an abundant and cheap material, its synthesis is rather simple and does not require toxic ions such as cobalt or nickel, its eventual spill-out will not cause severe environmental pollution. Further, the choice of a water-based suspension goes too in the direction of a more sustainable commercialization of future liquid cybernetic systems. Having dealt with several formulations, some of them hydrocarbon-based, we understood that this particular formulation, featuring polarizability of the surfactant molecules in a water environment, of course stabilizes

2211406 (7 of 10)

**ADVANCED
SCIENCE NEWS**

www.advancedsciencenews.com

**ADVANCED
MATERIALS**

www.advmat.de

the nanoparticles in the solvent and allows for a 3D reconfiguration of molecules and nanoparticles in a volume triggered by an electric field. This is like featuring an adaptive, electrically programmable routing of the equivalent network: an electric stimulus changes the coordination degree and the routing, as much as a pH variation was shown to induce ferroelectricity (i.e., the feature of producing electrical polarization via oriented domains) in an otherwise neutral liquid.[26]

The main advantage of the current device resides in its fluidity and unique amorphous nature. In principle, it provides robustness against impulsive mechanical shock, electrical shock, and ionizing radiation as well, while solid state devices (especially on glass/silicon substrates) are much more sensitive. Crystalline lattices can be severely damaged by electrical breakdown, mechanical cleavage, and also radiation-induced recrystallization or spallation, phenomena that are not likely to influence a liquid. In the case of a water-based FF, excessive voltage applied across the reservoir may only result in water electrolysis, which, due to gas evolution, may disturb the liquid computer only temporarily, with a full functional recovery once the voltage surge is removed. The results reported in Section S12, Supporting Information, represent a first demonstration of such advanced self-healing properties. Other two important features resulting from the fluidity of this colloid system are the non-necessity of a forming procedure (which instead limits the performance of solid filamentary memristors) and memory volatility. This, although disqualifies a FF as a permanent memory, opens nevertheless a pathway to reservoir computing. Usually memristive system is read with DC pulses, which might disturb stored information, as every DC interaction with a memristor may result is a Faradaic process of filament growth/disintegration, or charge trapping at the interface. On the other hand, an RF readout approach, so far that has been never applied, provides milder readout conditions and causes less interference to the sample.

In view of the reported features, we can conclude that further investigations using multiple ports and holonomic concepts[8] and further engineering steps toward a complex computer are possible, based on the spatial arrangement of the ports (see Section S15, Supporting Information). While the generation of DC voltage (at high impedance) can be easily implemented using low-complexity circuit solutions, read-out custom electronic circuits can take advantage of the demonstrated cumulative ultra-wide band impedance variation of the colloid, without necessarily requiring accurate frequency synthesis. The power required by the FF to run the in-memory computing scheme of Figure 3 is below 200 µW (Section S14, Supporting Information). Although the FF system cannot reach the power consumption of in-memory solid-state spiking neural networks architectures of nW orders,[27] the obtained value demonstrates low-power operation, compatible with those of microcontrollers. The energy consumption of in-memory computing, however, strongly depends on the type of processing executed. Moreover, solid-state devices are deeply miniaturized and their operation can regard few atomic layers of matter, while here the volume of the colloid is macroscopic, thus pertaining a nanoparticle system (roughly 10^{18} particles) rather than to a single nanoparticle domain, leaving room for important improvements. Given the demonstrated scaling capabilities, it is definitely interesting to investigate op-

eration using micrometric volumes of liquid containing a small number of nanoparticles.

In conclusion, we have demonstrated the first ever evidence of a FF in-memory computing system. An FF can be considered as both a device and a system and implement complex calculations both with custom in-memory computing schemes, and PRC, thus widening its spectrum of features. Besides extending the possibilities of already existing applications of FFs, these findings make solutions featuring unprecedented plasticity, fault-tolerance and resilience toward extreme environments a plausible reality, thanks to their amorphous nature.

6. Experimental Section

Conditions: All measurements were performed in an electronic laboratory environment at room temperature (unless otherwise specified) and they were executed mostly at night time to avoid possible vibrations that might occur in the laboratory during normal working hours.

Ferrofluid: An EMG601P ferrofluid, FerroTec, Lot Number U021920A was used.[28] The quantity of liquid used was 5 mL, that had been released in the vial using a pipette (unless otherwise indicated).

Vial: The vial was made of an inert acrylonitrile butadiene styrene (ABS) material while the electrical contacts, directly in contact with the liquid, were based on feed-lines of gold plated RF connectors, therefore not contributing to any chemical reaction. The vial (3 cm diameter) had been prepared to host RF sub-miniature version A (SMA) connectors (Wurth Elektronik, 1.6 mm straight printed circuit board (PCB), Manufacturer number 60314202124525) feed lines. The ground pins of the connectors had been cut to expose only the feed line of the connector. The vial had been drilled to host symmetrically the two feed lines. Finally, the connectors had been threaded in the drilled surface of the vial and fixed in place using a rubber band and hot glue. In order not to let the liquid evaporate, the vial needed to be closed using the supplied cap.

It was specifically chosen not to implement RF shielding on the vial to avoid undercut propagation modes, therefore permitting the observation of the phenomena without constraints.

Vector Network Analyzer: A PicoVNA 106 (300 kHz–6 GHz), Pico Technology, UK, had been used to read out the status of the material, using its built-in dynamic link libraries (DLL) under Microsoft Windows 7. In these experiments, the RF power used to perform the frequency sweep by the VNA is −3 dBm, and any significant impact of such a signal on the internal status evolution of the liquid was not observed. The number of measurement points was 201.

Bias Tee: The two bias tees used were commercial TCBT-14+, Mini Circuits (10 MHz–10 GHz), that had been soldered on two custom PCBs designed to be mounted on the RF mini enclosure RF-ENCL-MINI-NF-01, Gquipment.

DC Generator: The DC generator was implemented using a Micropython Board V1.1, connected, through its two available digital to analog converters (DACs) to an evaluation board of a Maxim OpAmp with an internal charge pump (MAX 44267 EVAL KIT) to generate, starting from a single 12 V supply, a ± 10 V DC signal using both INAP and INAM terminals. The DACs of the Micropython board had been set through the internal firmware to a high current drive. The Micropython board implemented a Virtual COM Port (VCP) interface to the personal computer so that the measurement program could set the output DC voltage on-demand by asynchronously sending commands to the module. The DC generator accepted an external power supply (GBC 34.0106.10, 18.5 W, 0.8 A at 12 V) that generated the 12 V supply required for the OpAmp to operate.

Measurement Software: The measurement software was run on a Windows 7 Virtual Machine, installed on a CentOS 7 control domain. Both VNA and DC generator were connected to the PC using USB cables.

To reproduce the measurements presented in the manuscript, it was sufficient to write a program that coordinated both VNA and DC generator to read out the S-parameters from the liquid and set the DC bias point. In this work, however, a specific Python scripting language that executes and compiles specific experiment files was designed.

Impedance Parameters Calculation: To calculate the impedance parameters starting from the S-parameters the following equations (Equations (1)–(4)) were used

$$Z_{11} = \frac{(1 + S_{11})(1 - S_{22}) + S_{21}S_{12}}{\Delta_S} Z_0 \tag{1}$$

$$Z_{12} = \frac{2S_{12}}{\Delta_S} Z_0 \tag{2}$$

$$Z_{21} = \frac{2S_{21}}{\Delta_S} Z_0 \tag{3}$$

$$Z_{22} = \frac{(1 - S_{11})(1 + S_{22}) + S_{21}S_{12}}{\Delta_S} Z_0 \tag{4}$$

where $\Delta_S = (1 - S_{11})(1 - S_{22}) - S_{21}S_{12}$. The above equations outputs were the impedance complex number values over frequency, from which magnitude values could be extracted. In this measurement system, these calculations were computed during the S-parameters measurements, but they can be calculated offline. Z_0 was assumed as $Z_0 = 50\ \Omega$. In these tests, the contribution of the vial was not eliminated and its full impedance contribution including the colloid was considered.

DC Characterization and Controlled Temperature Tests: The DC characterization was obtained using a Keithley 2635A—picoamperometer and nanovoltmeter. The temperature tests were run by using a Binder MK53 climatic chamber, by staging both vial, RF cables, and bias tee inside. The remainder part of the setup was kept outside the chamber.

PRC Readout Neural Network: The neural network was implemented in `tensorflow`. Training was achieved using 50 sequences of digits 0–3 obtained using the same measurement conditions of the other tests (see Section S11, Supporting Information). The optimizer used for training was `Adam` and all the layers had a sigmoid activation function. The "reset" sequence was not considered in the training, and only the 64 impedance values resulting from serialization were used. During the real-time inference the measurement system streams the data once all the pixels were serialized, that is, when a single digit iteration was finished, though the user datagram protocol (UDP) over an Ethernet physical layer. The inference was run on a PC where the trained model was loaded and the UDP packets were received from the network.

Measurements Processing and Graphs: All the results of this manuscript (except from the PicoVNA 106 that comes with its proprietary DLL and the vial that was rendered using PTC Creo), was obtained using open source software, that is Python, Inkscape (https://inkscape.org), Xfig (http://mcj.sourceforge.net), TeXMaker (https://www.xm1math.net/texmaker/) and Gimp (https://www.gimp.org). The files generated by the measurement system was processed, collated, and organized for plotting and visualization using custom `matplotlib` Python utilities.

Statistical Analysis: The impedance measurements reported here were acquired by collecting a massive amount of data for over 6 months, and for the reservoir computing dataset the statistical analyses (mean, standard deviation and histograms) reported in Section S11, Supporting Information, obtained using Python were run. The data in the confusion map of Figure 4B was obtained by post-processing measurements results using a custom Python script.

Supporting Information

Supporting Information is available from the Wiley Online Library or from the author.

Conflict of Interest

The authors declare no conflict of interest.

Data Availability Statement

The data that support the findings of this study are available from the corresponding author upon reasonable request.

[1] A. Adamatzky, *Unconventional Computing – A Volume in the Encyclopedia of Complexity and Systems Science*, Springer, New York **2018**.
[2] A. Adamatzky, *Handbook Of Unconventional Computing (In 2 Volumes)*, World Scientific, Singapore **2021**.
[3] A. Emch, *Am. Math. Mon.* **1901**, *8*, 10.
[4] A. Adamatzky, *Philos. Trans. R. Soc., B* **2019**, *374*, 20180372.
[5] N. R. Kheirabadi, A. Chiolerio, K. Szaciłowski, A. Adamatzky, *ChemPhysChem* **2022**, *24*, 202200390.
[6] A. Chiolerio, M. Quadrelli, *Adv. Sci.* **2017**, *4*, 1700036.
[7] A. Chiolerio, M. Quadrelli, *Energy Technol.* **2019**, *7*, 1800580.
[8] A. Chiolerio, *Adv. Intell. Syst.* **2020**, *2*, 2000120.
[9] V. N. Manoharan, *Science* **2015**, *349*, 1253751.
[10] S. Zhao, J.-Y. Zhang, Y. Fu, S. Zhu, H. C. Shum, X. Liu, Z. Wang, R. Ye, B. Z. Tang, T. P. Russell, Y. Chai, *Nano Lett.* **2022**, *22*, 5538.
[11] D. Ielmini, H.-S. P. Wong, *Nat. Electron.* **2018**, *1*, 333.
[12] N. Verma, H. Jia, H. Valavi, Y. Tang, M. Ozatay, L.-Y. Chen, B. Zhang, P. Deaville, *IEEE Solid-State Circuits Mag.* **2019**, *11*, 43.
[13] M. Le Gallo, A. Sebastian, R. Mathis, M. Manica, H. Giefers, T. Tuma, C. Bekas, A. Curioni, E. Eleftheriou, *Nat. Electron.* **2018**, *1*, 246.
[14] A. Sebastian, M. Le Gallo, R. Khaddam-Aljameh, E. Eleftheriou, *Nat. Nanotechnol.* **2020**, *15*, 529.
[15] N. Laleni, T. Soliman, F. Mueller, S. Mojumder, T. Kirchner, M. Lederer, T. Hoffmann, A. Guntoro, N. Wehn, T. Kaempfe, in *MikroSystemTechnik Congress*, VDE Verlag, Frankfurt **2021**, pp. 1–4.
[16] K. Nakajima, I. Fisher, *Reservoir Computing. Theory, Physical Implementations, and Applications*, Springer Nature, Singapore **2021**.
[17] E. Wlaźlak, D. Przyczyna, R. Gutierrez, G. Cuniberti, K. Szaciłowski, *Jpn. J. Appl. Phys.* **2020**, *59*, SI0801.
[18] S. P. Adhikari, M. P. Sah, H. Kim, L. O. Chua, *IEEE Trans. Circuits Syst. I* **2013**, *60*, 3008.

**ADVANCED
SCIENCE NEWS**

www.advancedsciencenews.com

**ADVANCED
MATERIALS**

www.advmat.de

[19] J. Shank, M. Tellekamp, M. Wahila, S. Howard, A. Weidenbach, B. Zivasatienraj, L. Piper, W. A. Doolittle, *Sci. Rep.* **2018**, *8*, 12935.

[20] L. Gonon, J.-P. Ortega, *Neural Networks* **2021**, *138*, 10.

[21] D. Przyczyna, M. Lis, K. Pilarczyk, K. Szaciłowski, *Molecules* **2019**, *24*, 2738.

[22] Y. Zhong, J. Tang, X. Li, B. Gao, H. Qian, H. Wu, *Nat. Commun.* **2021**, *12*, 408.

[23] X. Zhu, Q. Wang, W. D. Lu, *Nat. Commun.* **2020**, *11*, 2439.

[24] M. Zaheer, Y. Cai, A. B. Waqas, S. F. Abbasi, G. Zhu, C. Cong, Z.-J. Qiu, R. Liu, Y. Qin, L. Zheng, L. Hu, *Phys. Status Solidi RRL* **2020**, *14*, 2000050.

[25] H. Sato, H. Shima, T. Nokami, T. Itoh, Y. Honma, Y. Naitoh, H. Akinaga, K. Kinoshita, *Front. Nanotechnol.* **2021**, *3*, 660563.

[26] A. Chiolerio, T. Draper, C. Jost, A. Adamatzky, *Adv. Electron. Mater.* **2019**, *5*, 1900202.

[27] F. Moro, E. Hardy, B. Fain, T. Dalgaty, P. Clémençon, A. De Prà, E. Esmanhotto, N. Castellani, F. Blard, F. Gardien, T. Mesquida, F. Rummens, D. Esseni, J. Casas, G. Indiveri, M. Payvand, E. Vianello, *Nat. Commun.* **2022**, *13*, 3506.

[28] Ferrotec – EMG 600P Series Safety Datasheet, https://ferrofluid.ferrotec.com/wp-content/uploads/sites/3/emg600psds.pdf (accessed: May 2023).